Çukurova Üniversitesi
Mühendislik Fakültesi Dergisi
Çukurova University
Journal of the Faculty of Engineering
ISSN: 2757-9255 CİLT/VOLUME: 39 SAYI/ISSUE: 4 ARALIK/DECEMBER 2024

The Impact of Conjugate Heat Transfer in Flow Over a Vertical Plate and Application of Artificial Neural Network

Pınar YAĞLICA [1,a], **Özdeş ÇERMİK** [1,b]

[1]*Kahramanmaraş Sütçü İmam University, Faculty of Engineering-Architecture, Department of Mechanical Engineering, Kahramanmaraş, Türkiye*

[a]***ORCID****0000-0001-5736-4911;* [b]***ORCID****: 0000-0001-9308-4589*

Article Info
Received : 08.07.2024
Accepted : 23.12.2024
DOI: 10.21605/cukurovaumfd.1605967

Corresponding Author
Pınar YAĞLICA
pyaglica@gmail.com

Keywords
Conjugate heat transfer
Magnetic field
Keller box technique
Viscous dissipation
Artificial neural network

How to cite: *YAĞLICA, P., ÇERMİK, Ö., (2024). The Impact of Conjugate Heat Transfer in Flow Over a Vertical Plate and Application of Artificial Neural Network. Cukurova University, Journal of the Faculty of Engineering, 39(4), 907-922.*

ABSTRACT

Heat conduction properties are important in the flow area for the simulation of engineering applications where heat transfer is needed between both liquid and solid. Conjugate Heat Transfer (CHT) refers to thermal problems involving both conduction within the wall and convection within the fluid. CHT is crucial for heat exchangers, gas turbine blades, nuclear reactor cooling pipes, aircraft engines, and spacecraft. Additionally, the influence of the magnetic field is significant in fields such as electrostatic precipitation, MHD power generators and pumps, aeroheating, and polymer science. The motivation for this study is to understand the combined effects of CHT, mixed convection, magnetic fields, and viscous dissipation on velocity, temperature profiles, local skin friction, and heat transfer parameters over a vertical plate. The boundary layer equations have been derived from the Navier-Stokes and energy equations using similarity methods and solved numerically with the Keller Box technique. A new correlation for local skin friction and heat transfer parameters has been developed. Moreover, Artificial Neural Network (ANN) models have been applied to forecast desired numerical values. The optimal ANN model for local heat transfer has one hidden layer and nine neurons, achieving an R^2 value of 0.9077607 and an MSE of 0.0003101. For local skin friction, the best-performing model has one hidden layer and fifteen neurons, with an R^2 value of 0.9470261 and an MSE of 0.0250369.

Düşey Bir Plaka Üzerinde Olan Akışa Bileşik Isı Transferinin Etkisi ve Yapay Sinir Ağları Uygulaması

Makale Bilgileri
Geliş : 08.07.2024
Kabul : 23.12.2024
DOI: 10.21605/cukurovaumfd.1605967

Sorumlu Yazar
Pınar YAĞLICA
pyaglica@gmail.com

Anahtar Kelimeler
Birleşik ısı transfer
Manyetik alan
Keller box tekniği
Viskoz yayılım
Yapay sinir ağları

Atıf şekli: *YAĞLICA, P., ÇERMİK, Ö., (2024). The Impact of Conjugate Heat Transfer in Flow Over a Vertical Plate and Application of Artificial Neural Network. Cukurova University, Journal of the Faculty of Engineering, 39(4), 907-922.*

ÖZ

Isı iletim özellikleri, hem sıvı hem de katı arasında ısı transferinin gerektiği mühendislik uygulamalarının simülasyonu için akış alanında önemlidir. Birleşik Isı Transferi (CHT), duvar içinde iletim ve sıvı içinde taşınım içeren termal problemleri ifade eder. CHT, ısı değiştiricileri, gaz türbini kanatları, nükleer reaktör soğutma boruları, uçak motorları ve uzay araçları için büyük öneme sahiptir. Ayrıca, manyetik alanın etkisi elektrostatik çökeltme, MHD güç jeneratörleri ve pompaları, aeroısıtma ve polimer bilimi gibi alanlarda önemlidir. Bu çalışmanın amacı, birleşik ısı transferi (CHT), karışık taşınım, manyetik alan ve viskoz yayılmanın, düşey bir plaka üzerindeki hız, sıcaklık profilleri, yerel yüzey sürtünmesi ve ısı transferi parametreleri üzerindeki etkilerini anlamaktır. Sınır tabakası denklemleri, Navier-Stokes ve enerji denklemlerinden benzerlik yöntemleri kullanılarak elde edilmiş ve Keller Box tekniği ile sayısal olarak çözülmüştür. Yerel yüzey sürtünmesi ve ısı transferi parametreleri için yeni bir korelasyon geliştirilmiştir. Ayrıca, istenen sayısal değerleri tahmin etmek için Yapay Sinir Ağı (YSA) uygulanmıştır. Yerel ısı transferi için en uygun YSA modeli, bir gizli katman ve dokuz nörona sahip olup, R^2 değeri 0.9077607 ve MSE değeri 0.0003101 olarak elde edilmiştir. Yerel yüzey sürtünmesi için en iyi model ise bir gizli katman ve on beş nöron ile R^2 değeri 0.9470261 ve MSE değeri 0.0250369 olarak belirlenmiştir.

1. INTRODUCTION

Conjugate Heat Transfer (CHT) is a complex phenomenon that addresses the simultaneous interaction of heat transfer mechanisms within a solid and fluid. This complex process plays a pivotal role in numerous engineering applications, such as heat exchangers, fin structures, microelectronic chip cooling systems, furnaces, arc welding processes, and nuclear air pipes. A comprehensive understanding of CHT is essential for effectively designing and optimizing various thermal systems and components [1]. CHT problems have been investigated by several researchers. In non-porous normal flow conditions, Miyamoto et al. [2] imposed constant temperature and heat flux on the outer surface of the vertically oriented plate, examining the phenomenon of natural convection heat transfer. Char et al. [3] made a numerical analysis to investigate CHT effect on a moving plate with a specified velocity. Chang [4] numerically conducted a study for the natural convection and heat transfer characteristics within a vertically oriented, thin, conductive, and hollow circular cylinder transporting micropolar fluid. The equations were transformed into nonlinear form, and the resulting equations were solved using the finite difference method. Mamun et al. [5] studied the impact of heat generation on vertical flat plate. The Nonlinear equations were solved using the Keller Box technique and the results were obtained for various values of the heat conduction and conjugate heat transfer parameters, and Prandtl number.

Magnetohydrodynamics (MHD) has emerged as a prominent research area owing to its significance in numerous technological and industrial applications. These applications encompass areas such as MHD power generators and pumps, aeroheating, plasma analysis, and cooling of nuclear reactors. Various studies have been conducted on the flow of electrically conductive viscous fluids under the influence of a magnetic field, exploring different geometries. Afify [6] investigated the impacts of several parameters on a non-Darcy MHD problem. Das [7] examined thermal radiation, partial slip, and fluid properties that change with temperature on MHD flow and heat transfer over a flat plate. Mamun and Chowdhury [8] studied the impact of the magnetic field, viscous energy distribution, and heat generation on the incompressible, viscous, and electrically conductive liquid flow over a vertical flat surface considering the influence of conduction (conductive electricity). Chamka and Ben-Nakhi [9] investigated heat and mass transfer via MHD mixed convection in a non-Darcian porous medium taking into account the presence of a magnetic field, thermal radiation, and Soret and Dufour effects.

Artificial Neural Network (ANN) is a field of artificial intelligence that aims to simulate the learning and problem-solving abilities of computer systems. ANN provides computer systems with the ability to learn by using mathematical and statistical approaches that model the neural networks of the human brain. These networks are used to recognize and learn patterns in datasets. ANN has been used in many applications, such as image and language processing, game strategy development, and automated driving technologies. Due to their ability to work with large amounts of data and recognize complex patterns, ANN has the potential to provide effective solutions in various industries and problem domains [10]. ANN has been used by many researchers in heat transfer problems. Abad et al. [11] employed ANN and particle swarm optimization to forecast a heat and mass transfer problem. The use of ANN modeling in the context of heat transfer applications, including thermal issues, heat exchangers, and gas-solid fluidized beds was explored by Kamble et al. [12]. Using ANN in the studies, the prediction of parameters is enhanced, providing more accurate and reliable results compared to conventional numerical methods.

In this study, the effects of conjugate heat transfer, mixed convection, magnetic field, and viscous dissipation on velocity and temperature profiles, local skin friction, and heat transfer parameters have been evaluated for a vertical plate. A new correlation has been developed for local skin friction and heat transfer parameters. Furthermore, artificial neural networks have been employed to predict the required numerical values.

2. ANALYSIS

In this study, it is assumed that there is a two-dimensional, steady laminar flow over a thin vertical plate with a finite thickness (b) and length (L), (where $L >> b$). The schematic of the problem is shown in Figure 1. At a certain distance from the right surface of the plate, the free stream velocity and temperature are denoted as u_∞ and T_∞, respectively. The left surface of the plate is kept at a constant temperature T, (where $T_0 > T$). The study investigates the flow over the plate considering the effects of a magnetic field and

viscous dissipation. The properties of the fluid including thermal conductivity, viscosity, permeability, and specific heat are constant for the analysis.

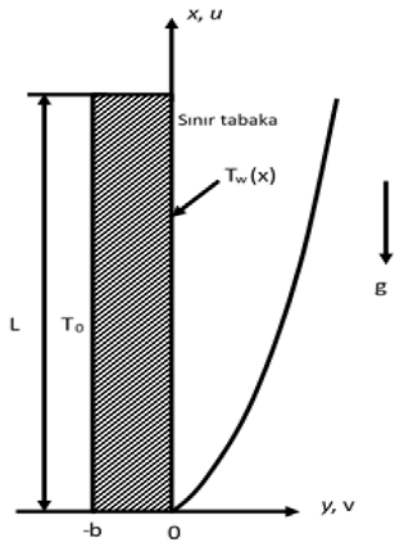

Figure 1. The schematic of the problem

The equations of the general boundary layer under these assumptions are modified to include the magnetic field effect while considering laminar and steady states. The Navier-Stokes equations in laminar and steady regimes are written using the Boussinesq and Non-Darcy approaches as follows [13].

$$\frac{\partial u}{\partial x}+\frac{\partial v}{\partial y}=0 \tag{1}$$

$$u\frac{\partial u}{\partial x}+v\frac{\partial u}{\partial y}=\upsilon\frac{\partial^2 u}{\partial y^2}+g\beta(T-T_\infty)-\frac{\sigma {B_0}^2}{\rho}(u-u_\infty) \tag{2}$$

$$u\frac{\partial T}{\partial x}+v\frac{\partial T}{\partial y}=\upsilon\frac{\partial^2 T}{\partial y^2}+\frac{\sigma {B_0}^2}{\rho Cp}(u-u_\infty)^2+\frac{\upsilon}{Cp}\left(\frac{\partial u}{\partial y}\right)^2 \tag{3}$$

The given equations are referred to as the extended Brinkman–Forchheimer-Darcy equations [14]. ν donates the kinematic viscosity, g represents gravitational acceleration, B_0 is the magnetic flux density, ρ is the fluid density, β stands for the thermal expansion coefficient, and T indicates the fluid temperature within the thermal boundary layer.

Boundary conditions for external flow are given below;

$$\begin{aligned} &x=0,\quad y>0 \rightarrow \mathrm{T}=\mathrm{T}_\infty,\ \ \mathrm{u}=\mathrm{u}_\infty \\ &x>0,\quad y=0 \rightarrow \mathrm{T}=\mathrm{T}_w(\mathrm{x}),\ \ \mathrm{u}=0,\ \ \mathrm{v}=0 \\ &y\rightarrow\infty \quad\rightarrow\quad \mathrm{T}\rightarrow\mathrm{T}_\infty,\ \ \mathrm{u}\rightarrow\mathrm{u}_\infty \end{aligned} \tag{4}$$

w is wall and ∞ is the boundary layer edge. Tw(x) that varies with x is the temperature of the plate surface.

Boundary conditions for the temperature distribution are given below;

$$\left.\frac{d^2T}{dy^2}\right|=0 \quad 0\le x\le L\ ;\ -\mathrm{b}<y<0. \tag{5}$$

The plate boundary conditions are as follows;

$$y = -b \;\rightarrow\; \mathrm{T_s} = T_0$$

$$T_s = T(x, r_0)\;; \quad -k_s \left.\frac{dT}{dy}\right|_{y=0,s} = -k_f \left.\frac{\partial T(x,0)}{\partial y}\right|_{y=0,f} \tag{6}$$

Here, k_s is the thermal conductivity coefficient for the plate while k_f is the fluid. The dimensionless expressions to solve the problem are given in Equation as follows [15]

$$\xi = \frac{x}{L},\ \eta = y\left(\frac{u_\infty}{\upsilon x}\right)^{1/2},\quad \psi(x,y) = (\upsilon u_\infty x)^{1/2} f(\xi,\eta),\quad \theta = \frac{T - T_\infty}{T_0 - T_\infty} \tag{7}$$

ψ(x, y) is free flow function. When these dimensionless expressions are used, the following velocity expressions are formed.

$$u = \frac{\partial \psi}{\partial y} = u_\infty f' \tag{8}$$

$$v = -\frac{\partial \psi}{\partial x} = -\left(\frac{u_\infty \upsilon}{x}\right)^{1/2}\left\{\frac{1}{2} f + \xi \frac{\partial f}{\partial \xi} - \frac{\eta}{2} f'\right\} \tag{9}$$

The obtained velocity components are substituted into the expressions in Equations (2) and (3), resulting in the following equations.

$$u\frac{\partial u}{\partial x} = u_\infty f' \frac{\partial u_\infty f'}{\partial x} = u_\infty^{\,2} f'\left[\frac{\partial f'}{\partial \xi}\frac{\partial \xi}{\partial x} + \frac{\partial f'}{\partial \eta}\frac{\partial \eta}{\partial x}\right] = u_\infty^{\,2} f'\left[\frac{1}{L}\frac{\partial f'}{\partial \xi} - \frac{\eta}{2x} f''\right] \tag{10}$$

When Equation (10) is utilized and rearranged, Equation (11) is obtained.

$$u\frac{\partial u}{\partial x} = \frac{u_\infty^{\,2}}{x}\left[\xi f' \frac{\partial f'}{\partial \xi} - \frac{\eta}{2} f f''\right] \tag{11}$$

$$v\frac{\partial u}{\partial y} = -\frac{u_\infty^{\,2}}{x}\left\{\frac{1}{2} f f'' + \xi f'' \frac{\partial f}{\partial \xi} - \frac{\eta}{2} f f''\right\} \tag{12}$$

$$\frac{v}{r}\frac{\partial}{\partial r}\left(r\frac{\partial u}{\partial r}\right) = \frac{\upsilon}{r}\left(\frac{u_\infty}{2x}\frac{u_\infty}{2x}\right)^{1/2} u_\infty \frac{1}{2}\frac{\partial}{\partial \eta}\left(\frac{r^2 - r_0^{\,2}}{r_0}\right)\frac{r}{r_0} f'' = \frac{u_\infty^{\,2}}{x}\left\{(1 + \lambda\eta) f''\right\}' \tag{13}$$

$$\frac{\upsilon \partial^2 u}{\partial y^2} = \frac{u_\infty^{\,2} f'''}{x} \tag{14}$$

$$g\beta(T - T_\infty) = g\beta\theta\,(T_0 - T_\infty) \tag{15}$$

$$\frac{\sigma B_0^{\,2}}{\rho}(u - u_\infty) = \frac{\sigma B_0^{\,2}}{\rho} u_\infty \left[f' - 1\right] \tag{16}$$

When the expressions in Equations (11-12-13-14-15-16) are substituted into Equation (2), the following momentum equation is obtained.

$$f''' + \frac{1}{2} f f'' - \frac{\sigma B_0^{\,2} x}{\rho u_\infty}(f' - 1) + g\beta\theta\frac{(T_0 - T_\infty)x}{u_\infty^{\,2}} = \xi\left\{f'\frac{\partial f'}{\partial \xi} - f''\frac{\partial f}{\partial \xi}\right\} \tag{17}$$

If the above equation is rearranged using the dimensionless expressions, $Ha = \frac{\sigma {B_0}^2 {r_0}^2}{\mu}$, $\mathrm{Re} = \frac{u_\infty r}{\upsilon}$, $Mn = \frac{Ha}{\mathrm{Re}}$, $Ri = \frac{Gr}{\mathrm{Re}^2}$, $Gr = \frac{g\beta(T_0 - T_\infty)L^3}{\upsilon^2}$, $x = L\xi$ the final form of the momentum equation (Equation 18) is obtained.

$$f''' + \frac{1}{2} ff'' - Mn\xi(f' - 1) + Ri\theta\xi = \xi\left\{ f' \frac{\partial f'}{\partial \xi} - f'' \frac{\partial f}{\partial \xi} \right\} \tag{18}$$

In the momentum equation; Ri is the Richardson number, indicating the extent to which natural and forced convection occur. Ri → 0 implies that forced heat transfer dominates completely, while Ri → ∞ implies that natural convection is entirely effective. The Richardson number does not vary as a function of x. Grashof (Gr), Reynolds (Re) and Prandtl (Pr) numbers are used in the equations [16].

If adjustments are made to the Energy Equation (Equation 3), where utilizing the dimensionless expression $\theta = \frac{T - T_\infty}{T_0 - T_\infty}$ from Equation (7), the following expressions are first written one by one;

$$u\frac{\partial T}{\partial x} = \frac{u_\infty (T_0 - T_\infty)}{x}\left[\xi f' \frac{\partial \theta}{\partial \xi} - \frac{\eta}{2}\theta' f' \right] \tag{19}$$

$$v\frac{\partial T}{\partial y} = -\frac{u_\infty (T_0 - T_\infty)}{x}\left[\frac{1}{2} f\theta' + \xi\theta' \frac{\partial f}{\partial \xi} - \frac{\eta}{2}\theta' f' \right] \tag{20}$$

$$\frac{\upsilon}{\mathrm{Pr}} \frac{\partial^2 T}{\partial y^2} = \frac{u_\infty (T_0 - T_\infty)}{x} \frac{1}{\mathrm{Pr}} \theta'' \tag{21}$$

$$\frac{\sigma {B_0}^2}{\rho Cp}(u - u_\infty)^2 = \frac{\sigma {B_0}^2}{\rho Cp} {u_\infty}^2 (f' - 1)^2 \tag{22}$$

$$\frac{\upsilon}{Cp}\left(\frac{\partial u}{\partial y} \right)^2 = \frac{\upsilon}{Cp}\left(\frac{\partial u_\infty f'}{\partial \eta} \right)^2 \left(\frac{\partial \eta}{\partial r} \right)^2 = \frac{{u_\infty}^2}{Cp}(f'')^2 \left(\frac{u_\infty}{x} \right) \tag{23}$$

Equations (18-19-20-21-22) are substituted into the Energy Equation (Equation 3), and Equation (24) is obtained as follows;

$$\frac{1}{\mathrm{Pr}}\theta'' + \frac{1}{2} f\theta' + \frac{\sigma {B_0}^2 x u_\infty}{\rho Cp(T_0 - T_\infty)}\left(f'^2 - 1 \right) + \frac{{u_\infty}^2}{Cp(T_0 - T_\infty)}(f'')^2 = \xi\left\{ f' \frac{\partial \theta}{\partial \xi} - \theta' \frac{\partial f}{\partial \xi} \right\} \tag{24}$$

In addition to the dimensionless expressions used for the Momentum Equation, when the expression for $Ec = \frac{{u_\infty}^2}{Cp(T_0 - T_\infty)}$ is also used in Equation (24), the final form of the Energy Equation is obtained.

$$\frac{1}{\mathrm{Pr}}\theta'' + \frac{1}{2} f\theta' + MnEc\xi(f'^2 - 1) + Ec(f'')^2 = \xi\left\{ f' \frac{\partial \theta}{\partial \xi} - \theta' \frac{\partial f}{\partial \xi} \right\} \tag{25}$$

3. NUMERICAL SOLUTION

The momentum and energy equations, represented by Equations (18) and (25), have been numerically resolved using the Keller Box technique. The impact of various parameters on local skin friction and heat transfer has been analyzed. Correlations have been developed for local skin friction and heat transfer. Both parameters have been optimized using ANN modeling based on the obtained data, determining the most

suitable model. The Keller Box technique is defined as an alternative closed (implicit) method. This method possesses several favorable characteristics for solving all parabolic partial differential equations. The principal characteristics of this method and the path to follow for the solution have been defined by Cebeci. The Keller-Box technique involves slightly more arithmetic compared to the Crank-Nicolson method for solving equations. It provides second-order accuracy in irregular x and y intervals and allows for very rapid variations in x. It facilitates the easy programming of the solution for numerous coupled equations. The Keller Box technique is implemented by following the steps. Firstly, the equation or equations are reduced to first order. Secondly, central difference methods are employed to formulate finite difference equations. Thirdly, if not linear, algebraic result equations are linearized and expressed in matrix form. Finally, the linear system is with block-tridiagonal elimination method [17].

Firstly, the equations are expressed in the form of a system of secondary equations.

$$f' = u\,,\; u' = v\,,\; g = \theta\,,\; g' = p \tag{26}$$

Using Equation (26), the momentum and energy equations are rearranged and written in finite difference form as follows;

$$h_j^{-1}\left[v_j^n - v_{j-1}^n\right] + \left(\frac{1}{2}+\alpha_n\right)(fv)_{j-1/2}^n + Ri\,\xi(g)_{j-1/2}^n - Mn\,\xi(u)_{j-1/2}^n - \alpha_n\left[(u^2)_{j-1/2}^n - (v)_{j-1/2}^{n-1}(f)_{j-1/2}^n + (v)_{j-1/2}^n(f)_{j-1/2}^{n-1}\right] = R_{j-1/2}^{n-1} \tag{27}$$

$$\frac{1}{\Pr}h_j^{-1}\left[p_j^n - p_{j-1}^n\right] + \left(\frac{1}{2}+\alpha_n\right)(fp)_{j-1/2}^n + MnEc\xi(u^2)_{j-1/2}^n + Ec(v^2)_{j-1/2}^n - \alpha_n\begin{bmatrix}(ug)_{j-1/2}^n - u_{j-1/2}^n g_{j-1/2}^{n-1} + u_{j-1/2}^{n-1} g_{j-1/2}^n \\ + f_{j-1/2}^{n-1} p_{j-1/2}^n - f_{j-1/2}^n p_{j-1/2}^{n-1}\end{bmatrix} = T_{j-1/2}^{n-1} \tag{28}$$

Equation (27) $R_{j-1/2}^{n-1}$ and Equation (28) $T_{j-1/2}^{n-1}$ are expressed as follows;

$$R_{j-1/2}^{n-1} = -L_{j-1/2}^{n-1} - \alpha_n\left[(fv)_{j-1/2}^{n-1} - (u^2)_{j-1/2}^{n-1}\right] \tag{29}$$

$$T_{j-1/2}^{n-1} = -M_{j-1/2}^{n-1} + \alpha_n\left[(fp)_{j-1/2}^{n-1} - (ug)_{j-1/2}^{n-1}\right] \tag{30}$$

If Equations (27) and (28) are rearranged in the form of Equation (31) (Newton linearization), Equations (32) and (33) are written as follows;

$$f_j^n = f_j^i + \delta f_j^i \tag{31}$$

$$h_j^{-1}\left[\delta v_j^i - \delta v_{j-1}^i\right] + \left(\frac{1}{2}+\alpha_n\right)(\delta fv)_{j-1/2}^i + Ri\,\xi(\delta g)_{j-1/2}^i - Mn\,\xi(\delta u)_{j-1/2}^i - \alpha_n\left[(\delta u^2)_{j-1/2}^i - (v)_{j-1/2}^{n-1}(\delta f)_{j-1/2}^i + (\delta v)_{j-1/2}^i(f)_{j-1/2}^{n-1}\right] = (r_2)_j^i \tag{32}$$

$$\frac{1}{\Pr}h_j^{-1}\left[\delta p_j^i - \delta p_{j-1}^i\right] + \left(\frac{1}{2}+\alpha_n\right)(\delta fp)_{j-1/2}^i + MnEc\xi(\delta u^2)_{j-1/2}^i + Ec(\delta v^2)_{j-1/2}^i - \alpha_n\begin{bmatrix}(\delta ug)_{j-1/2a}^i - \delta u_{j-1/2}^i g_{j-1/2}^{n-1} + u_{j-1/2}^{n-1}\delta g_{j-1/2}^i \\ + f_{j-1/2}^{n-1}\delta p_{j-1/2}^i - \delta f_{j-1/2}^i p_{j-1/2}^{n-1}\end{bmatrix} = (r_3)_j \tag{33}$$

The Keller Box technique is then used to solve Equations (32) and (33) after linearization.

Table 1. Comparison of local heat transfer parameters with Pr=10, Ri=7.9, p=Mn=Ec = 0.0

ξ	Lloyd and sparrow	Chang	Present study
0.00000	0.7281	0.7280	0.7278
0.00125	0.7313	0.7291	0.7318
0.00500	0.7404	0.7373	0.7403
0.01250	0.7574	0.7566	0.7574
0.05000	0.8259	0.8351	0.8289
0.12500	0.9212	0.9412	0.9397
0.50000	1.0290	1.0603	1.0601

The works of Lloyd and Sparrow [18] and Chang [19] have been compared with the current technique to confirm the accuracy, and the results show a good agreement as illustrated in Table 1.

4. RESULTS AND DISCUSSION

In this research, the combined effects of heat transfer and magnetic field on the flow over a flat plate have been investigated. The equations and parameters obtained through the numerical method are written in a Fortran program. The influence of parameters on local friction and heat transfer is determined for the mixed heat transfer parameter (Ri) =0.01, 0.1, 1.0, 5.0, 10.0, the combined heat transfer parameter (p) = 0.0, 0.1, 0.2, 0.3, the magnetic field parameter (Mn) = 0.5, 1.0, 1.5, 2.0, the Eckert number (Ec) = -0.1, -0.05, 0, 0.05, 0.1, Re = 250, and Pr = 1. The conjugated heat transfer parameter p=0 corresponds to the limit case of an isothermal wall, and the value of p indicates the extent of the wall's heat conduction effect [4].

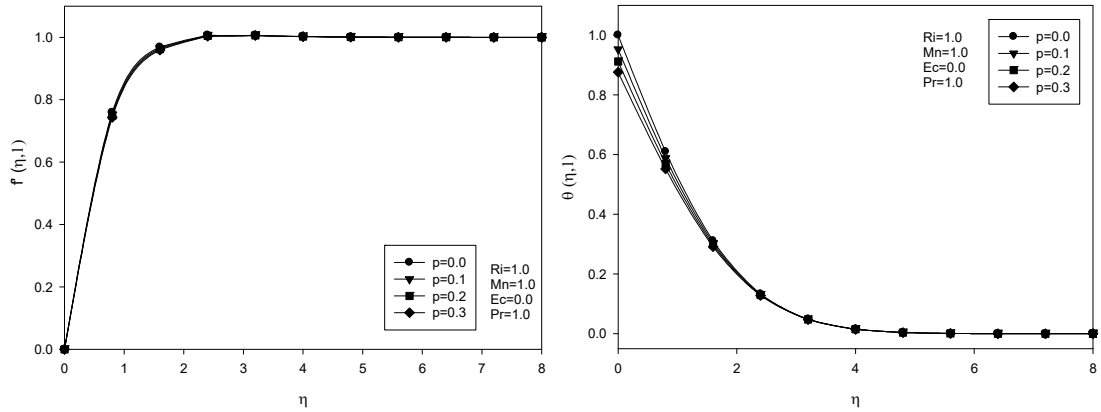

(a) (b)

Figure 2. Velocity (a) and temperature (b) for various p

Figure 2 depicts the influence of the parameter p on the velocity and temperature profiles within the thermal boundary layer. The values are obtained for the case of Ri=Mn=Pr=1.0 and Ec=0.0. As the conjugated heat transfer p increases, the velocity and temperature gradients on the wall decrease. A decrease in plate conductivity (ks) or an increase in fluid conductivity (kf) along with the parameter p increases the temperature difference between the inner and outer surfaces. Solid-fluid temperature decreases due to the constant temperature of the outer surface [19].

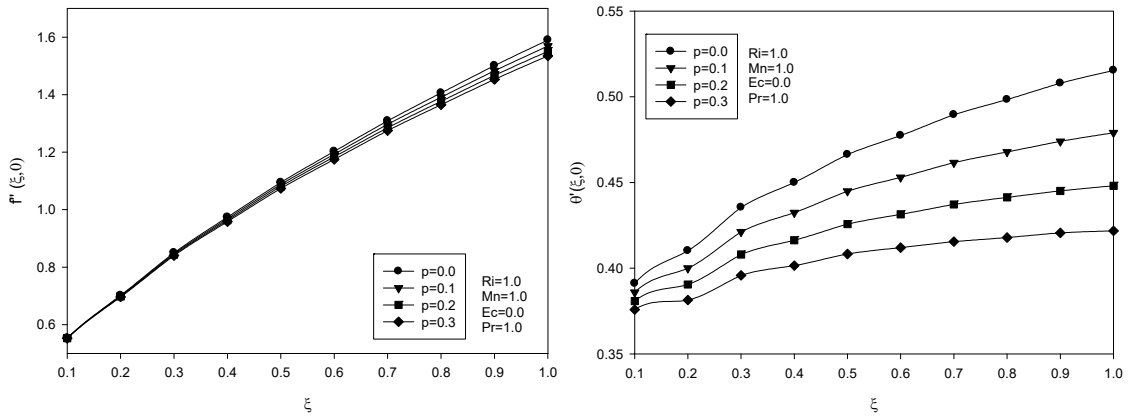

(a) (b)

Figure 3. Effects of p on the local skin friction (a) and the local heat transfer (b) parameters

Figure 3 depicts the variations of local skin friction coefficient and heat transfer parameters with p and ξ. An increase in parameter p results in a decrease in the values of local friction coefficient and local heat transfer parameters. Additionally, the increase in fluid temperature on the plate with ξ results in an increase in local friction and heat transfer parameters with ξ. This is attributed to the increased lift force effect due to the rising interface temperature along the flow direction, consequently increasing the surface friction factor [4].

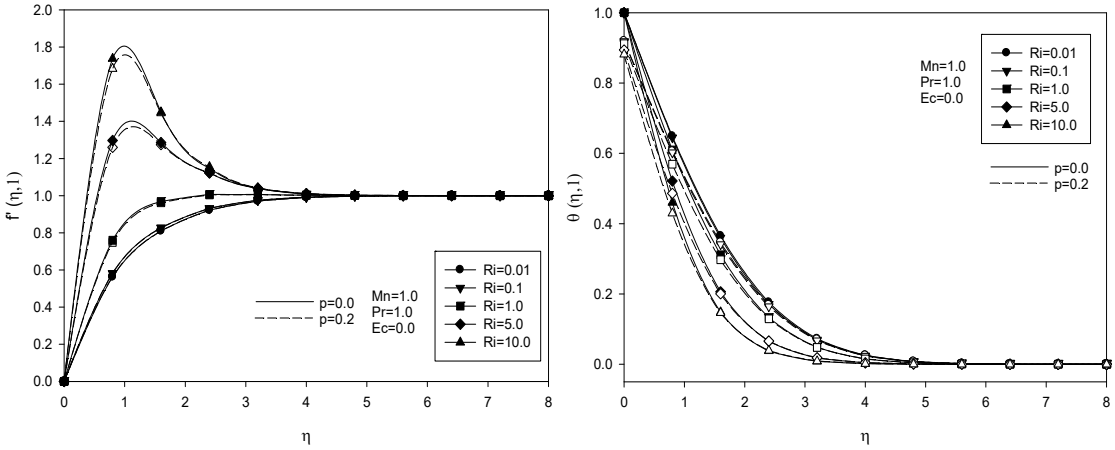

(a) (b)

Figure 4. Velocity (a) and temperature (b) profiles for various Ri

Figure 4 represents the effect of different Ri values on velocity and temperature profiles. The values are obtained for Mn=1.0, Ec=0.0, and Pr=1.0. It is investigated for different *Ri* values for both the isothermal plate (p=0.0) and the non-isothermal plate (p=0.2>0). As *Ri* increases, lift forces become more effective, enhancing the velocity profile within the boundary layer. However, the temperature profile decreases with an increase in the parameter Ri. This observation holds true for both isothermal and non-isothermal conditions, as depicted in the graphs.

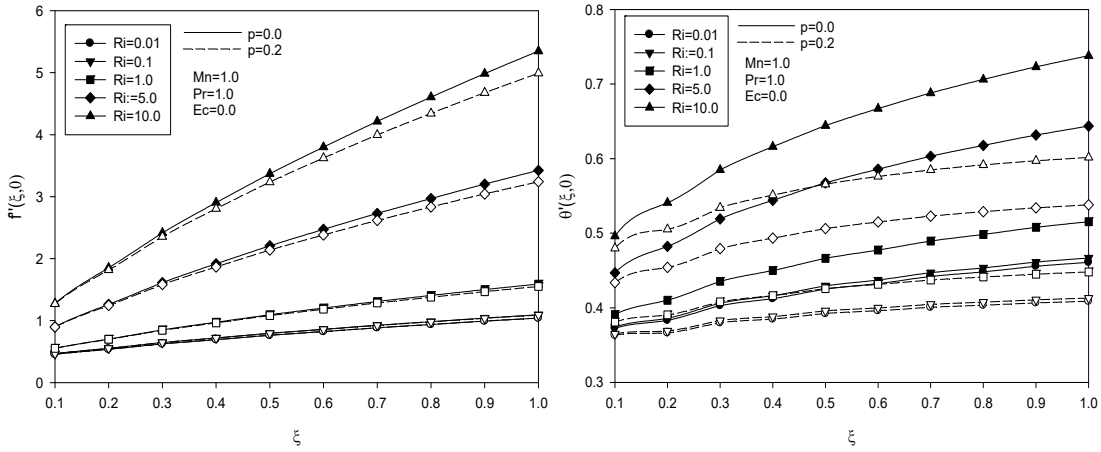

(a) (b)

Figure 5. Effects of Ri on the local skin friction (a) and the local heat transfer (b) parameters

In Figure 5, the variations of local friction and local heat transfer parameters along the plate are given for both the isothermal and non-isothermal cases. In Figure 5a, the change in the local friction coefficient with the mixed heat transfer parameter *Ri* is shown. In both cases, the local friction coefficient for the plate increases with *Ri*. This is attributed to the increase in lift force effects in mixed heat transfer, leading to accelerated fluid flow and an increase in local friction coefficient. Figure 5b presents the change in the local heat transfer parameter with the mixed heat transfer parameter *Ri*. An increase in *Ri* has elevated the local heat transfer parameter for both the isothermal (p=0.0) and non-isothermal (p=0.2) plates. This is due to the increased lift forces, accelerating fluid velocity, and consequently enhancing the local heat transfer effect [4].

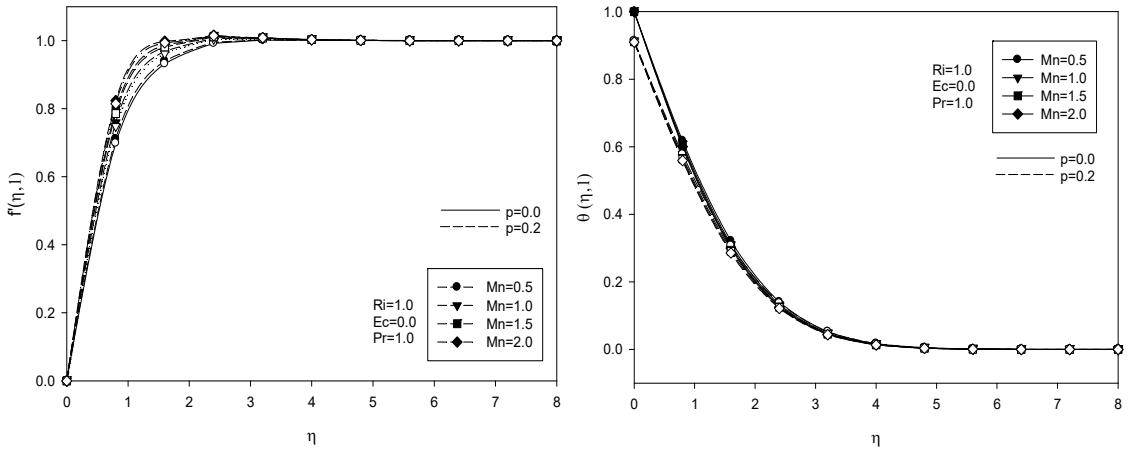

(a) (b)

Figure 6. Velocity (a) and temperature (b) profiles for various Mn

Figure 6 illustrates the impact of Mn on the velocity (a) and temperature (b) profiles. The values are obtained for Ri= Pr=1.0 and Ec=0.0. It is investigated for different *Mn* values for isothermal and non-isothermal plates.

An increment in *Mn* enhances the velocity and temperature profiles. The increase in the magnetic field intensifies the flow concentration, and thus, the magnetic force of the medium and the flow resistance caused by the delaying effect of the opposite direction, resisting the flow [9]. As seen in Figure 6 shows that increasing the magnetic field parameter Mn enhances both the velocity and temperature gradients at the wall.

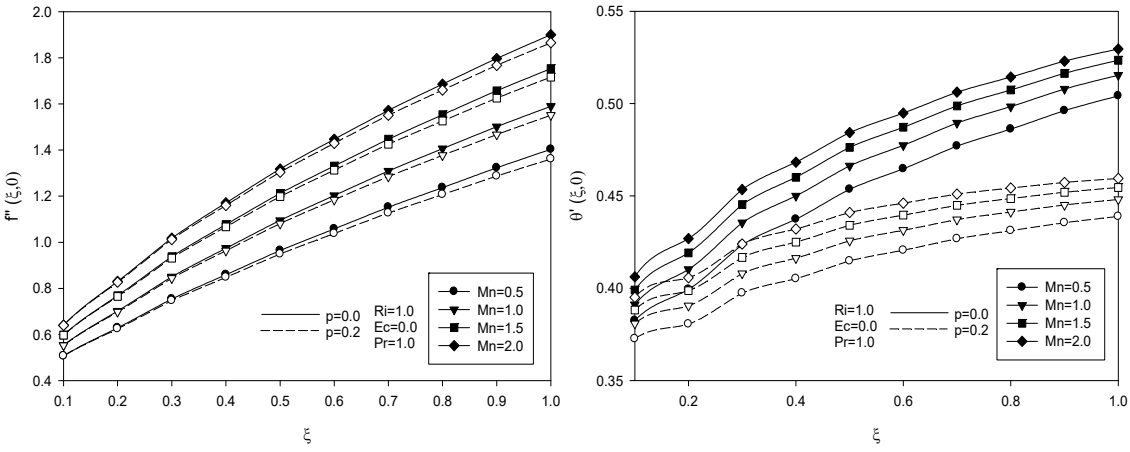

(a) (b)

Figure 7. Effects of Mn and p on the local skin friction (a) and the local heat transfer (b) parameters

In Figure 7, the variations of local friction and heat transfer parameters along the interior of the plate are given for both isothermal and non-isothermal plate conditions. An increase in the magnetic field parameter enhances local friction and local heat transfer parameters. The magnetic force is against the flow and reduces the wall shear stress. Increasing the Mn value also reduces the interface temperature [8] and the heat transfer reduces with the decrease of Mn as shown in Figure 7b.

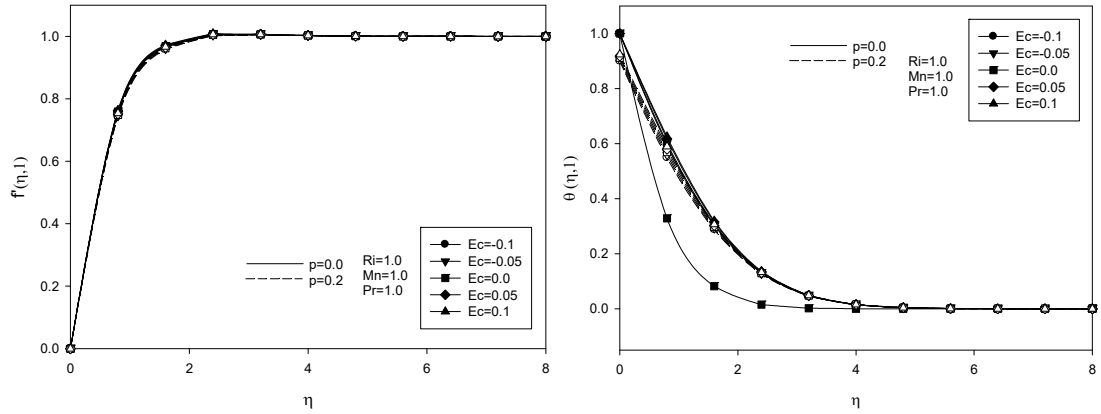

(a) (b)

Figure 8. Velocity (a) and temperature (b) for various Ec

The effect of the Eckert number (*Ec*) on the dimensionless velocity (a) and temperature (b) profiles within the boundary layer is shown in Figure 8. The values are obtained for Ri=1.0, Mn=1.0, and Pr = 1.0. It is investigated for different *Ec* values for both the isothermal and non-isothermal plates.

An increment in the Eckert number enhances the velocity profile. For a positive value of *Ec*, there is heat transfer from the plate to the fluid since The plate's temperature exceeds that of the free stream. Viscous dissipation results in heat generation within the fluid, leading to an increased temperature distribution in the flow region. This occurs because heat energy is retained in the liquid due to viscous heating. As the liquid temperature rises, the temperature gradient decreases. As seen in Figure 8b, the impact of *Ec* on temperature is in the opposite direction.

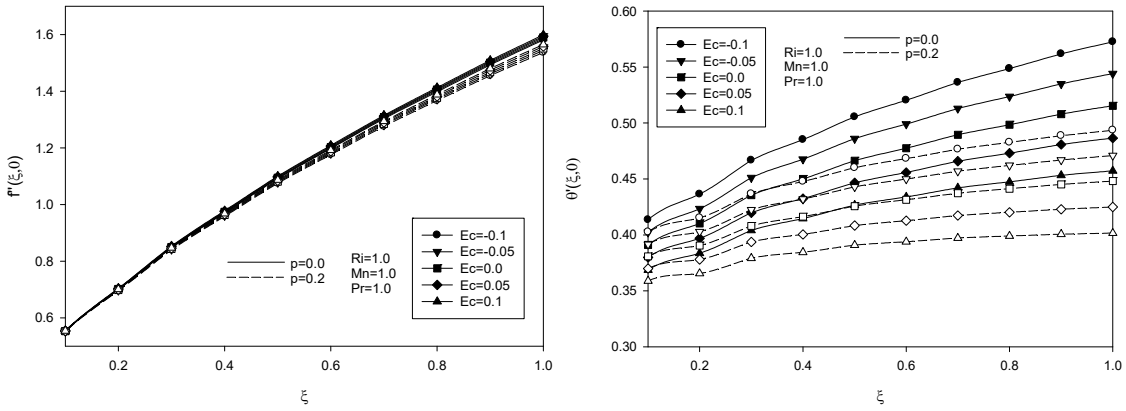

(a) (b)

Figure 9. Impact of Ec and p on the local skin friction (a) and the local heat transfer (b) parameters

In Figure 9, the variations of local skin friction and heat transfer parameters along the plate are presented for isothermal and non-isothermal plate conditions.

Viscous dissipation acts as a heat generation source within the fluid. The Eckert number represents an assisting effect for negative values and creates a counter effect on heat transfer for positive values [21]. With the increase in the Eckert number (*Ec*), local friction increases, while local heat transfer decreases.

5. CORRELATION

Correlations were established by conducting regression analysis using SPSS based on the obtained data. Regression analysis enables modeling the relationship between dependent and independent variables, measuring the magnitude of the relationship between these variables [22].

Regression analysis for heat transfer values was conducted using the SPSS program based on the obtained data. The results of the regression analysis, conducted without squaring the parameters affecting local heat transfer, are presented in Figure 10, and Equation (34) is derived.

$$\theta'(\xi,0) = 0.349 + 0.137\,\xi - 0.199\,p + 0.017\,Ri + 0.017\,Mn - 0.359\,Ec \tag{34}$$

In Equation (34), $R^2 = 0.848$ and the standard error = 0.02762 are obtained.

Model Summary

Model	R	R Square	Adjusted R Square	Std. Error of the Estimate	Change Statistics	
					R Square Change	F Change
1	,921[a]	,848	,846	,02762	,848	386,040

Coefficients[a]

Model		Unstandardized Coefficients		Standardized Coefficients	t	Sig.
		B	Std. Error	Beta		
1	(Constant)	,349	,006		55,705	,000
	VAR00001	,137	,005	,616	29,397	,000
	VAR00002	-,199	,014	-,292	-13,940	,000
	VAR00003	,017	,001	,579	27,584	,000
	VAR00004	,017	,005	,071	3,361	,001
	VAR00005	-,359	,037	-,202	-9,632	,000

Figure 10. The SPSS analysis for the local heat transfer parameter

The regression analysis including the squares of parameters influencing local heat transfer is conducted, and Figure 11 presents the result. Equation (35) is obtained through regression analysis using the SPSS program. The correlation coefficients and determination coefficients for local heat transfer are found to be the same program.

$$\theta'(\xi,0) = 0.314 + 0.301\xi - 0.164\xi^2 - 0.248p + 0.223p^2 + 0.028Ri - 0.001Ri^2 + 0.019Mn - 0.001Mn^2 - 0.359Ec + 0.161Ec^2 - 0.012Ec^3 \tag{35}$$

In Equation (35), an R^2 value of 0.899 and a standard error of 0.02273 are obtained.

Model Summary

Model	R	R Square	Adjusted R Square	Std. Error of the Estimate	R Square Change	Ch F Change
1	,948[a]	,899	,896	,02273	,899	274,518

a. Predictors: (Constant), VAR00011, VAR00010, VAR00002, VAR00003, VAR00007, VAR00005, VAR00006, VAR00008

Coefficients[a]

Model		Unstandardized Coefficients		Standardized Coefficients	t	Sig.	95,0% Confidence Interval for B	
		B	Std. Error	Beta			Lower Bound	Upper Bound
1	(Constant)	,314	,013		23,606	,000	,288	,340
	VAR00001	,301	,014	1,354	21,117	,000	,273	,329
	VAR00002	-,164	,014	-,766	-11,951	,000	-,191	-,137
	VAR00003	-,248	,052	-,364	-4,817	,000	-,350	-,147
	VAR00004	,223	,231	,073	,965	,335	-,232	,678
	VAR00005	,028	,002	,967	12,532	,000	,024	,033
	VAR00006	-,001	,000	-,396	-5,122	,000	-,002	-,001
	VAR00007	,019	,021	,080	,909	,364	-,022	,059
	VAR00008	-,001	,008	-,011	-,121	,904	-,016	,014
	VAR00009	-,359	,092	-,202	-3,894	,000	-,540	-,177
	VAR00010	,161	,382	,008	,420	,674	-,591	,912
	VAR00011	-,012	10,217	,000	-,001	,999	-20,109	20,085

a. Dependent Variable: VAR00012

Figure 11. The SPSS analysis for the local heat transfer parameter with square values

Using the obtained data, regression analysis for local friction values was also conducted in the SPSS program. The regression analysis without squaring the parameters affecting local friction yielded the results presented in Figure 12, and equation (36) was derived.

$$f''(\xi,0) = -0.140 + 1.465\,\xi - 0.124\,p + 0.237\,Ri + 0.214\,Mn + 0.056\,Ec \tag{36}$$

In equation (36), the coefficient of determination (R^2) is 0.851, and the standard error is 0.30888.

Model Summary

Model	R	R Square	Adjusted R Square	Std. Error of the Estimate	R Square Change	Ch… F Change
1	,922[a]	,851	,848	,30888	,851	394,024

a. Predictors: (Constant), VAR00005, VAR00004, VAR00001, VAR00002, VAR00003

Coefficients[a]

Model		Unstandardized Coefficients B	Unstandardized Coefficients Std. Error	Standardized Coefficients Beta	t	Sig.	Correlations Zero-order	Correlations Partial
1	(Constant)	-,140	,070		-2,004	,046		
	VAR00001	1,465	,052	,585	28,131	<,001	,585	,834
	VAR00002	-,124	,160	-,016	-,775	,439	-,030	-,042
	VAR00003	,237	,007	,713	34,256	<,001	,709	,879
	VAR00004	,214	,055	,081	3,885	<,001	,038	,204
	VAR00005	,056	,416	,003	,135	,893	,003	,007

a. Dependent Variable: VAR00006

Figure 12. SPSS analysis for the local skin friction parameter

The result of the regression analysis, based on the obtained data, with square terms affecting the local friction parameter, is presented in Figure 13, and equation (37) is derived.

$$f''(\xi,0) = -0.307 + 2.130\xi - 0.666\xi^2 - 0.225p + 0.456p^2 + 0.291Ri - 0.005Ri^2 + 0.250Mn - 0.014Mn^2 + 0.057Ec + 0.641Ec^2 - 0.036Ec^3 \tag{37}$$

In equation (37), R^2=0.858 and the Standard Error=0.30425 were obtained.

Model Summary

Model	R	R Square	Adjusted R Square	Std. Error of the Estimate
1	,926[a]	,858	,853	,30425

a. Predictors: (Constant), VAR00011, VAR00010, VAR00002, VAR00003, VAR00007, VAR00005, VAR00009, VAR00001, VAR00004, VAR00006, VAR00008

Coefficients[a]

Model		Unstandardized Coefficients B	Unstandardized Coefficients Std. Error	Standardized Coefficients Beta	t	Sig.
1	(Constant)	-,307	,178		-1,724	,086
	VAR00001	2,130	,191	,850	11,173	<,001
	VAR00002	-,666	,184	-,276	-3,625	<,001
	VAR00003	-,225	,690	-,029	-,327	,744
	VAR00004	,456	3,093	,013	,148	,883
	VAR00005	,291	,030	,878	9,587	<,001
	VAR00006	-,005	,003	-,168	-1,835	,067
	VAR00007	,250	,276	,094	,905	,366
	VAR00008	-,014	,103	-,014	-,138	,890
	VAR00009	,057	1,233	,003	,046	,963
	VAR00010	,641	5,111	,003	,126	,900
	VAR00011	-,036	136,749	,000	,000	1,000

a. Dependent Variable: VAR00012

Figure 13. SPSS analysis for the local skin friction parameter with square values

6. ARTIFICIAL NEURAL NETWORK

In this study, based on the results of numerical analysis, an effective model has been developed for local heat transfer and friction values. Determination coefficient (R^2) and Mean Squared Error (MSE) have been determined for the desired output values. The heat transfer parameter is the output, and p, Ri, Mn, and Ec are the inputs for the ANN application. All data has been appropriately divided into training, testing, and validation sets. Using the same testing, validation, and training data, an ANN model has been developed for different hidden layers and neurons. These models include one hidden layer with 3, 6, 9, 12, and 15 neurons and two hidden layers with 3, 6, 9, 12, and 15 neurons. Table 2 presents the R^2 and MSE values for different numbers of neurons and hidden layers. The performance of ANN models has been compared. As shown in the table, the highest R^2 and the lowest MSE values are achieved with one hidden layer and nine neurons. This model has been selected as the best-performing one, with an R^2 value of 0.9077607 and an MSE value of 0.0003101. Moreover, the determination coefficient R^2 is expected to be very close to 1.

Table 2. Different hidden layers and neuron numbers for R^2 and MSE values (Local heat transfer)

Hidden layer	Neurons	R^2	MSE
1	3	0.8169551	0.0006153
1	6	0.8559505	0.0004843
1	**9**	**0.9077607**	**0.0003101**
1	12	0.8537413	0.0004917
1	15	0.8412335	0.0005337
2	3	0.8108080	0.0006360
2	6	0.8215294	0.0006000
2	9	0.8275015	0.0005799
2	12	0.8272322	0.0005808
2	15	0.8216942	0.0005994

The values obtained from the ANN analyses provide very accurate results in numerical terms. The best ANN models for heat transfer are shown in Figure. As the iteration number increases, the loss and MSE values decrease. Figures 14 and 15 show the graphs of the best ANN model for heat transfer. The selected test data and predicted values from the dataset are very close to each other.

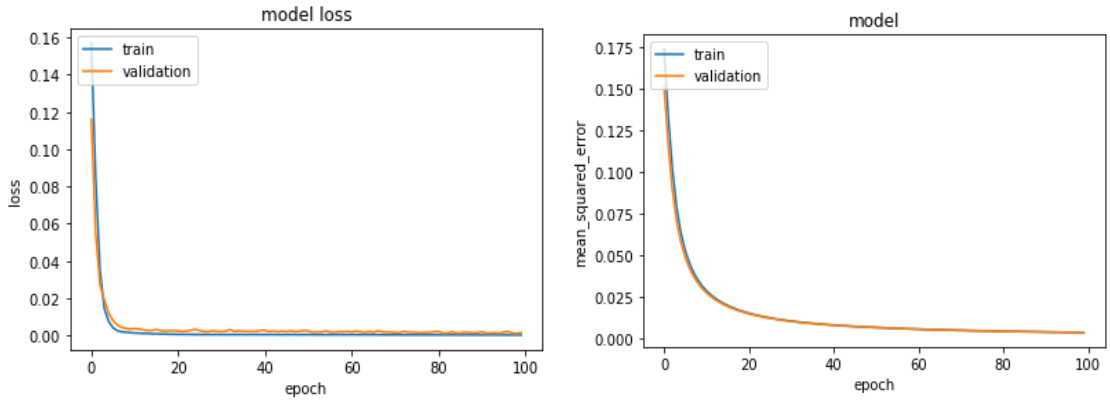

(a) (b)

Figure 14. Artificial neural network model (Local heat transfer)

Artificial Neural Network (ANN) is utilized to establish an effective model for the local skin friction parameter based on the results of numerical analyses. The determination coefficient (R^2) and mean square error values have been determined for the desired output parameters.

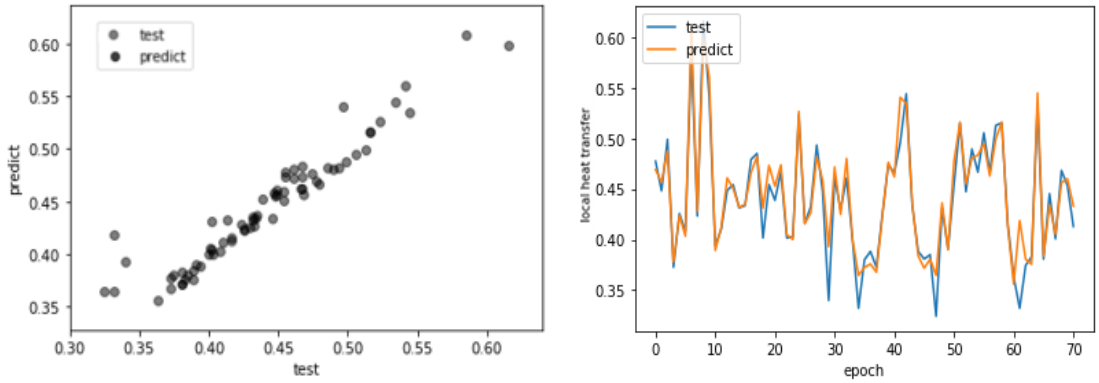

(a) (b)

Figure 15. Test and predicted values for local heat transfer in ANN

The input parameters for the ANN application are the local friction parameter, p, Ri, Mn, and Ec. All data were appropriately divided into training, validation, and test sets. A single hidden layer was created using different neuron numbers based on the same test, validation, and training data. These models encompassed one hidden layer with 3, 6, 9, 12, 15, 18, 24, and 27 neurons. Table 3 presents R^2 and MSE values for various neuron numbers. The performance of the ANN models is compared and the best model is selected based on the highest R^2 and lowest MSE values, which were achieved with one hidden layer and fifteen neurons. The R^2 value is 0.9470261, and the MSE value is 0.0250369.

Table 3. Different neuron numbers for R^2 and MSE values (Local skin friction coefficient)

Hidden layer	Neurons	R^2	MSE
1	3	0.8372382	0.0769258
1	6	0.8486468	0.0715337
1	9	0.9206943	0.0374821
1	12	0.9323556	0.0319706
1	**15**	**0.9470261**	**0.0250369**
1	18	0.9386864	0.0289785
1	24	0.9241009	0.0358720
1	27	0.9243456	0.0357564

In Figures 16 and 17, the graphical representations of the optimal ANN model for local friction are presented. The test data selected from the dataset and the corresponding predicted values exhibit a remarkable alignment, affirming the excellent concordance between the ANN model and the numerical results.

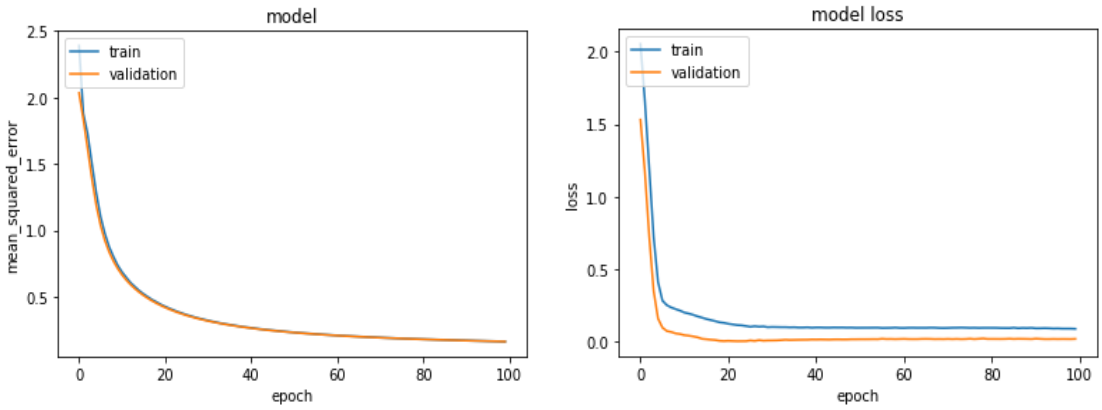

(a) (b)

Figure 16. Artificial neural network model (Local skin friction)

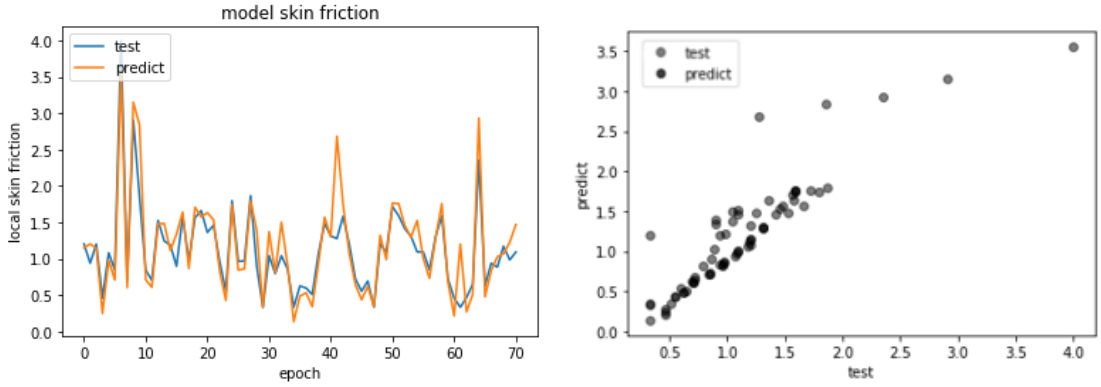

(a) (b)

Figure 17. Test and predicted values for local skin friction in ANN

The differences in MSE values between the ANN models and the figures may be due to differences in data sets, where training or validation data show lower MSE compared to test data. Additionally, variations in data distribution or evaluation conditions might explain the differences observed.

7. CONCLUSION

This investigation focuses on the flow over a vertical plate. The equations (Navier-Stoke and energy) have been converted into boundary layer equations through the utilization of the similarity method. These boundary layer equations have been solved numerically by employing the Keller Box technique. Ri, p, Mn parameters, and Ec number have been investigated for their effects on the velocity and temperature distributions in the boundary layer and local skin friction and heat transfer parameters. The findings revealed that an increase in the parameter p led to a reduction in both local skin friction and local heat transfer. Meanwhile, an escalation in the parameters Ri and Mn resulted in an augmentation of the effects on local friction and local heat transfer. Moreover, as the Ec increased, it intensified the influence on local friction while diminishing its effect on local heat transfer. Furthermore, Using the output data of the numerical method, a Neural Network (ANN) model compatible with the data was developed and optimized for both local skin friction and heat transfer. R^2 and MSE values were calculated to evaluate the performance of the model. The models with the highest R^2 and lowest MSE were chosen for local heat transfer and skin friction. After the parameter optimization, it was shown that the most appropriate model for local heat transfer has one hidden layer and nine neurons with 0.9077607 R^2 and 0.0003101 MSE values. For local skin friction, the most suitable model has one hidden layer and fifteen neurons with R^2 value of 0.9470261 and an MSE value of 0.0250369.

For future research, we plan to extend this study to different geometries and flow conditions to validate the robustness of the ANN models further. Additionally, the impact of varying magnetic fields, fluid properties, and more complex boundary conditions will be considered to enhance the applicability of the proposed models in real-world engineering problems. The integration of advanced machine learning techniques beyond ANN could also be explored to improve prediction accuracy and computational efficiency.

8. REFERENCES

1. Baytas, A.C., 2006. Transport in porous media. ITU Journal Science, 4(1), 3-13.
2. Miyamoto, M., Sumikawa, J., Akiyohi, T., Nakamura, T., 1980. Effects of axial heat conduction in a vertical flat plate on free convection heat transfer. Int. J. Heat Mass Transf., 23, 1545-1553.
3. Char, M.I., Chen, C.K., Cleaver, J.W., 1990. Conjugate forced convection heat transfer from a continuous, moving flat sheet. Int. J. Heat Fluid Fl., 11, 257-261.
4. Chang, C.L., 2008. Numerical simulation for natural convection of micropolar fluids flow along slender hollow circular cylinder with wall conduction effect. Communications in Nonlinear Science and Numerical Simulation, 13(3), 624-636.

5. Mamun, A.A., Chowdhury, Z.R., Azim, M.A., Maleque, M.A., 2008. Conjugate heat transfer for a vertical flat plate with heat generation effect. Nonlinear Analysis: Modelling and Control, 13(2), 213-223.
6. Afify, A.A., 2007. Effects of temperature-dependent viscosity with soret and dufournumbers on non-darcymhd free convective heat and mass transfer pasta vertical surface embedded in a porous medium. Transport in Porous Media, 66(3), 391-401.
7. Das, K., 2012. Impact of thermal radiation on mhd slipflow over a flat plate withvariable fluid properties. Heat and Mass Transfer, 48(5), 767-778.
8. Mamun, A.A., Chowdhury, Z.R., Azim, M.A., Molla, M.M., 2008. MHD-conjugate heat transfer analysis for a vertical flat plate in presence of viscous dissipation and heat generation. International Communications in Heat and Mass Transfer, 35(10), 1275-1280.
9. Chamkha, A.J., Ben-Nakhi, A., 2008. Mhd mixedconvection-radiation interactionalong a permeable surface immersed in a porous medium in the presence ofsoret and dufour's effects. Heat and Mass Transfer, 44(7), 845.
10. Oztemel, E., 2020. Yapay sinir ağları. Papatya Yayıncılık, İstanbul, 232.
11. Abad, J., Mohebbi, N., Alizadeh, R., Fattahi, A., Doranehgard, M.H., Alhajri, E., Karimi, N., 2020. Analysis of transport processes in a reacting flow of hybrid nanofluid around a bluff-bodyembedded in porous media using artificial neural network and particle swarm optimization. Journal of Molecular Liquids, 313.
12. Kamble, L.V., Pangavhane, D.R., Singh, T.P., 2014. Heat transfer studies using artificial neural network-a review. International Energy Journal, 14(1), 25-42.
13. Chamkha, A.J., Issa, C., Khanafer, K., 2002. Natural convection from an inclined plate embedded in a variable porosity porous medium due to solar radiation. International Journal of Thermal Sciences, 41(1), 73-81.
14. Lauriat, G., Ghafir, R., 2000. Forced convective heat transfer in porous media. Handbook of Porous Media, New York, 201-204.
15. Kaya, A., Aydın, O., 2009. The effect of radiation on forced convection flow around a wedge. Turkish Soc Thermal Sciences Technology, 29(1), 1-6.
16. Kaya, A., Aydin, O., 2014. Effects of buoyancy and conjugate heat transfer flowover on a vertical plate embedded in a porous media. Journal of Thermal Scienceand Technology, 34(1), 35-41.
17. Cebeci, T., 2002. Convective heat transfer. Springer, 357.
18. Lloyd, J.R., Sparrow, M., 1970. Combined force and free convection flow on vertical surfaces. Int. J. Heat Mass Tran., 13, 434-438.
19. Chang, C.L., 2006. Numerical simulation of micropolar fluid flow along a flat plate with wall conduction and buoyancy effects, J. Phys. D: Appl. Phys., 39, 1132-1140.
20. El-Kabeir, S.M.M., El-Hakiem, M.A., Rashad, A.M., 2008. Group method analysis of combined heat and mass transfer by MHD non-Darcy non-Newtonian natural convection adjacent to horizontal cylinder in a saturated porous medium. Applied Mathematical Modelling, 32(11), 2378-2395.
21. Aydın, O., Kaya, A., 2008. Non-Darcian forced convection flow of viscous dissipating fluid over a flat plate embedded in a porous medium. Transport in Porous Media, 73(2), 173-186.
22. Kilic, S., 2013. Linear regression analysis. Journal of Mood Disorders, 3(2), 90-92.